Continental Shelf Research 254 (2023) 104904

Contents lists available at ScienceDirect

Continental Shelf Research

journal homepage: www.elsevier.com/locate/csr

Long-term changes in ecosystem functioning of a coastal bay expected from a shifting balance between intertidal and subtidal habitats

Dunia Rios-Yunes [a,*,1], Justin C. Tiano [a,b,1,2,**], Pieter van Rijswijk [a], Emil De Borger [a], Dick van Oevelen [a], Karline Soetaert [a]

[a] Royal Netherlands Institute for Sea Research (NIOZ), Department of Estuarine and Delta Systems, 5 PO box 140, 4400 AC, Yerseke, the Netherlands
[b] Wageningen University & Research, the Netherlands

ARTICLE INFO

Keywords:
Ecosystem functioning
Intertidal zone
Biogeochemistry
Nutrients
Carbon
Organic matter

ABSTRACT

Coastal areas are subjected to several anthropogenic stressors with much of the world's intertidal areas receding due to human activities, coastal erosion and sea level rise. The Dutch Eastern Scheldt (ES) has been predicted to lose around 35% of intertidal areas by 2060. This study investigates differences between biogeochemical fluxes of intertidal and subtidal sediments of the ES and assesses how ongoing erosion may modify the sedimentary ecosystem functioning of this coastal bay in the coming decades. Monthly fluxes and porewater concentrations of dissolved inorganic nitrogen (DIN), phosphorous (DIP), silica (DSi), carbon (DIC) and oxygen (O_2) as well as organic matter (OM) characteristics were measured from intertidal and subtidal sediments from June 2016–December 2017. Compared to subtidal stations, OM was significantly more reactive in intertidal samples and exhibited 37% higher O_2 fluxes, suggesting a strong influence from microphytobenthos. Subtidal sediments exhibited an average efflux of nitrates (0.28 mmol m^{-2} d^{-1}) and phosphates (0.09 mmol m^{-2} d^{-1}) into the water column, while intertidal areas displayed average influxes (nitrates = −1.2 mmol m^{-2} d^{-1}, phosphates = −0.03 mmol m^{-2} d^{-1}) directed into the sediment. The calculated removal of total DIN and DIP from the water column was 34–38% higher in intertidal compared to subtidal samples suggesting stronger denitrification and phosphorus adsorption to solid particles from intertidal sediments. As an upscaling exercise, we estimate potential erosion induced changes if the ES stations are representative for the system. With this assumption, we estimate 11% and 8% reductions for respective nitrogen and phosphorus removal in the entire ES by 2060. Given the global observations of eroding intertidal areas and rising sea levels, we suggest that the predicted habitat loss may cause significant changes for coastal biogeochemistry and should be investigated further to understand its potential consequences.

1. Introduction

Coastal sediments are well known for their high primary production and importance in global biogeochemical cycling (Woodward, 2007) These habitats receive OM and nutrients from autochthonous (e.g., local algal blooms) and allochthonous sources (e.g., terrestrial including sewage and fertilizers; Gilbert et al., 2007) which enter the sediment by tidal action, sedimentation, and sediment reworking by benthic organisms (Arndt et al., 2013; Kang et al., 2015). Other essential ecosystem functions mediated by coastal sediments include the mineralization of organic matter (OM), bentho-pelagic nutrient exchange, as well as the cycling, and the export and/or removal of inorganic nutrients (Khalil et al., 2013; Lessin et al., 2018; Magalhães et al., 2002).

Nutrient exchange between the water column and the sediment is different between intertidal and subtidal regions. In intertidal sediments tidal flushing during inundation causes the release of porewater nutrients into the water column (Cabrita et al., 1999; Falcão and Vale, 1998; Rocha and Cabral, 1998), while nutrient exchange in permanently

* Corresponding author.
** Corresponding author. Royal Netherlands Institute for Sea Research (NIOZ), Department of Estuarine and Delta Systems, 5 PO box 140, 4400 AC, Yerseke, the Netherlands.
E-mail addresses: Dunia.Rios.Yunes@nioz.nl (D. Rios-Yunes), Justin.Tiano@wur.nl (J.C. Tiano).
[1] Dunia Rios-Yunes and Justin C. Tiano contributed equally to this work.
[2] Present address: Wageningen Marine Research, Wageningen University and Research, PO box 68, 1970 AB, IJmuiden, the Netherlands.

https://doi.org/10.1016/j.csr.2022.104904
Received 10 September 2022; Received in revised form 2 December 2022; Accepted 4 December 2022
Available online 17 December 2022

subtidal sediments is governed primarily by molecular diffusion (Falcão and Vale, 1998), faunal-induced sediment reworking and irrigation (Kristensen et al., 2012; Laverock et al., 2011), and wave-mediated advective transport ("subtidal pump", Riedl et al., 1972). The difference in biogeochemical cycling between intertidal and subtidal coastal areas may lead to distinct ecological functions allocated to each zone (De Borger et al., 2020). Moreover, there are ecosystem-specific differences (Herbert, 1999) that should be considered as for example subtidal denitrification has been reported to be higher than in the intertidal in some systems (Eyre et al., 2011; Joye and Paerl, 1993) and lower in others (Piehler and Smyth, 2011). The input of OM in intertidal sediments is mostly associated with local microphytobenthic blooms, while OM influxes in subtidal sediments rely more on pelagic deposition leading to potential differences in OM quality and carbon characteristics between tidal zones.

Coastal habitats have been gaining attention as areas for "Blue carbon" storage (i.e. organic carbon) (Byun et al., 2019; Hilmi et al., 2021; IUCN, 2021; Laffoley et al., 2014). Most of the focus, however, has been placed on vegetated areas and less is known about the role of pure sedimentary ecosystems. Reports of high organic carbon stocks stored in mudflats (Bulmer et al., 2020; Byun et al., 2019; Douglas et al., 2022) suggest the importance of certain sedimentary habitats for long term carbon sequestration. However, dynamics between tidal zones and the possible threat of coastal erosion and/or sea level rise (SLR) remains largely unexplored.

The balance between intertidal and subtidal sediments in coastal areas is in constant change. However, the extent of intertidal areas is decreasing worldwide as a consequence of land reclamation, land-use change, SLR, coastal hardening, coastal erosion and reduced sediment supply (Murray et al., 2019). Notably, erosion, decreased sediment input, and SLR will determine the loss of intertidal area and its conversion to subtidal areas (Murray et al., 2019; Ysebaert et al., 2016). This conversion may alter the ecosystem functions and services provided by these areas (e.g. nutrient recycling, export and removal), with potentially wider consequences to regional biogeochemistry.

An ongoing example of changing intertidal-subtidal dynamics can be found in the Eastern Scheldt (ES) tidal bay located in the southwest of The Netherlands. The ES was transformed from an estuary into a fully saline tidal bay upon the construction of a "storm-surge barrier" (Delta Works project) at its mouth and several riverine dams in 1986 (Smaal and Nienhuis, 1992). These developments decreased the likelihood of local flooding but drastically reduced natural sediment deposition while altering the biological, abiotic, morphodynamic and biogeochemical characteristics of the ES (Nienhuis and Smaal, 1994; Smaal and Nienhuis, 1992; tenBrinke, 1994; Wetsteyn et al., 2003). Decreased water column nutrient concentrations led to increased nutrient limitation to primary production (Smaal et al., 2013; Wetsteyn et al., 2003; Wetsteyn and Kromkamp, 1994) while the reduced sedimentation resulted in a loss of intertidal surface area (Smaal and Nienhuis, 1992).

A condition known as "sand starvation" is currently exhibited in the ES resulting from continuous erosion of intertidal areas, lower riverine input of sediments and weaker tidal currents that fail to replenish tidal flat sediments (van Zanten and Adriaanse, 2008; Ysebaert et al., 2016). By 2001, it was estimated that the ES had lost 8% (870 ha) of intertidal areas accounting for ~0.5 km^2 per year (van Zanten and Adriaanse, 2008). The ES continues to experience geomorphological and biogeochemical changes (Smaal and Nienhuis, 1992; Ysebaert et al., 2016) including the ongoing loss of intertidal flats (and associated ecosystem functions) and their conversion to subtidal areas.

The aim of this study was to assess biogeochemical characteristics of intertidal and subtidal ES sediments and to predict changes to ecosystem functions due to the expected conversion of intertidal to subtidal areas as a consequence of sand starvation. OM mineralization and nutrient fluxes were estimated for intertidal and subtidal sediments by conducting monthly sediment incubations over a period of 1.5 years.

2. Methods

2.1. Study area

The Eastern Scheldt is a tidal bay and former estuary located in the southwest of The Netherlands with a mean depth of 8.84 m. Its sedimentary habitats cover an area of 350 km^2, ~110 km^2 of which being intertidal areas (Jiang et al., 2019). It remains connected to the North Sea though sluices, resulting in a tidal flush dominated system (~2 × 10^4 m^3 s^{-1}) with a decreasing landward gradient of suspended chlorophyll *a* (chl a), nutrient concentrations, suspended sediment and turbidity (Smaal and Nienhuis, 1992; Wetsteyn and Kromkamp, 1994). Riverine input in the ES is negligible (4.3 m s^{-1}) (Jiang et al., 2019).

Sampling was conducted in three sedimentary sites from the ES intertidal: Zandkreek (ZK), Olzendenpolder (OP), and Dortsman (DT) and three sites from the subtidal: Hammen (HM), Viane (VN), and Lodijkse gat (LG). Intertidal samples from ZK (51.55354∘ N, 3.87278∘ E) exhibited silty sediments (median grain size under 62.5 μm) while OP (51.46694∘ N, 4.072694∘ E) and DT (51.56804∘ N, 4.01425∘ E) were characterized by very fine sand (62.5–125 μm) and fine sand (125–250 μm), respectively. Samples from HM (51.65607∘ N, 3.858717∘ E) displayed the coarsest sediments in the study and were taken from a depth of 7 m. The muddy subtidal site VN (51.60675∘ N, 3.98501∘ E) lies within a bathymetric depression (13 m depth) adjacent to intertidal **areas (Fig. 1).** LG (51.48463∘ N, 4.166001∘ E; 17 m depth) was the most inland location and exhibited very fine sand (Fig. 1).

The granulometric, and bioirrigation (the faunal mediated exchange of solutes into the sediment) characteristics, as well as, detailed information about macrofauna assemblages from these samples are documented in De Borger et al. (2020). Macrofaunal species densities at intertidal sites averaged 1 326, 1 955, 15 384 ind. m^{-2} corresponding to 17.0, 14.3, 7.3 g (ash free dry weight [AFDW]) of biomass per m^2 for sites ZK, OP and DT respectively. Abundances at intertidal sites were dominated numerically by *Hediste diversicolor* in ZK, *Peringia ulvae* in OP and *Corophium volutator* in DT. In comparison, subtidal sites HM, VN and LG all featured lower average densities (931, 168, and 580 ind. m^{-2}), but sandy stations (HM and LG) had higher biomass (36.4, 46.9 g AFDW m^{-2}) than VN (2.7 g AFDW m^{-2}; (De Borger et al., 2020). The numerically dominant species in the subtidal site HM was *Mytilus edulis*, while *Crepidula fornicata* and *Ophiura ophiura* displayed the highest abundances at LG and VN respectively.

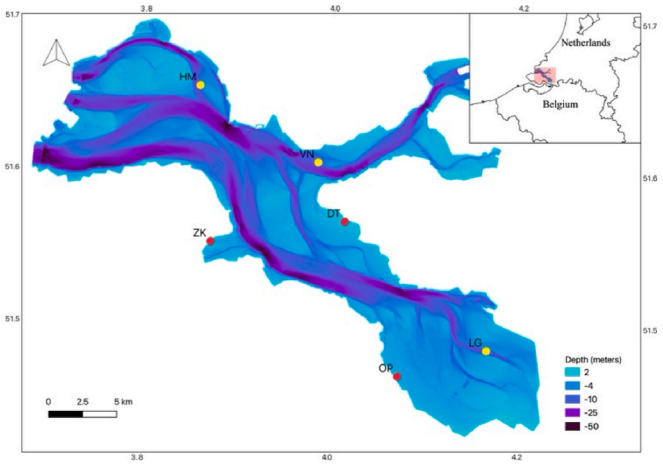

Fig. 1. Bathymetric map of the Eastern Scheldt showing sampling points in the intertidal (red): Zandkreek (ZK), Olzenderpolder (OP) and Dortsman (DT) and subtidal (yellow): Hammen (HM), Viane (VN) and Lodijkse gat (LG) zones.

2.2. Sample collection

Intact sediment core samples were collected monthly between June 2016 to December 2017 (exact sampling dates can be found in **Supplementary** Table A 1 **and** Table A 2) and used for porewater extraction and flux measurements of oxygen (O_2) and nutrients. Duplicate samples were taken for both intertidal and subtidal stations amounting to 114 and 102 cores from the intertidal and subtidal zones, respectively, as subtidal sampling was not possible in January and February of 2017 due to logistic constraints (**Supplementary** Table A 1). Sandy and muddy sites in the subtidal and intertidal stations were chosen to cover different sediments in contrasting environments.

Intertidal sediments were sampled during low tide and were defined between −2 and 2 m Normal Amsterdam Water Level ('NAP'; Kuijper and Lescinski, 2013). Cores for flux measurements were collected by inserting a cylindrical 14.5 cm diameter (∅) by 30 cm (height) transparent PVC pipe into the sediment at a depth of 15–20 cm and carefully extracting the sediment without disturbing or tilting the core. Subtidal samples were collected using a cylindrical box corer (30 cm ∅, 55 cm height) deployed from the RV *Delta*, from which subcores were obtained and ~30 L of surface water were pumped from each subtidal site for later use in the laboratory.

Additional cylindrical PVC cores (3 cm ∅, 20 cm height) were collected for porewater nutrient extraction (all months), dry sediment parameters (median grain size, carbon and nitrogen content, porosity; June and December of 2016), and solid phase phosphorus (solid-P) and iron (solid-Fe) (July and December of 2016 and 2017). These cores were inserted 10+ cm into the sediment to obtain two segments: shallow from 0 to 5 and deep from 5 to 10 cm depth. Samples for chl a, phaeophorbide, and phaeophytin measurements were extracted from the upper 1 cm of the sediment using a cut-off syringe (all months).

2.3. Dry sediment parameters

Details regarding the laboratory analysis of sediment grain size parameters, organic carbon (OC) and total nitrogen (TN) content, porosity calculation, and pigment extraction can be found in De Borger et al. (2020). Sediment data previously reported in De Borger et al. (2020) were combined with additional samples from the monitoring period and recalculated for the current study. Organic carbon percentages were combined with bulk density measurements to obtain OC stocks in the upper 10 cm of sediment.

The ratio chl a/(chl a + phaeophytin) was used as a proxy for organic matter reactivity as assessed with sediment pigments (Bonifácio et al., 2014; Lamarque et al., 2021; Pastor et al., 2011). For solid-P and solid-Fe extraction, a ~500 mg subsample of sediment was obtained within an anaerobic glove box. These samples were exposed to 10 mL of 65% nitric acid (HNO_3) and placed in a microwave to heat the sample (microwave energy is absorbed by the liquid surrounding the sample) while monitoring the temperature. The metals present were converted into soluble salts by the nitric acid and the high temperature (205°C), to prepare them for measurement via Inductive Coupled Plasma – Optical Emission Spectrometry (ICP-OES).

2.4. Porewater nutrients

Immediately after arrival to the lab, the porewater cores were placed inside an anaerobic glove box (Coy lab products, USA) to prevent aerobic chemical reactions prior to extraction. Thereafter, sediment from shallow and deep segments was collected in 50 mL centrifuge tubes (polypropylene; TPP, Switzerland). Porewater was extracted by centrifugation (10 min, 5000 rpm) (Sigma 3-18 KS, Sigma Laborzentrifugen GmbH, Germany). Extracted porewater (500 μL) was placed back in the anaerobic glove box and filtered (0.45 μm) into 6 mL plastic vials to be stored at −20°C for 2–5 days until analysis. For porewater phosphate, a separate 100 μL sample was acidified with 10 μL of hydrogen sulfide (H_2S) to inhibit sorption of PO_4^{3-} to other materials. Upon thawing, samples for NH_4^+, NO_2^-, NO_3^-, PO_4^{3-}, and DSi were analyzed by a SEAL QuAAtro segmented flow analyzer (Jodo et al., 1992). Detection limits were: 0.05 mmol m^{-3} for NH_4^+ and DSi, 0.03 mmol m^{-3} for NO_3^- and PO_4^{3-} and 0.01 mmol m^{-3} for NO_2^-.

2.5. Flux measurements

After collection, the 14.5 cm ∅ sediment cores were brought to a climate-controlled chamber at The Royal Netherlands Institute for Sea Research, Yerseke (NIOZ- Yerseke) which was set to represent the ambient water temperature (7–20 °C) in the Eastern Scheldt. Water temperatures in the ES were obtained from the Dutch Directorate-General for Public Works and Water Management (Rijkswaterstaat, n. d.). Each core was placed in a thermostatic bath, aerated, and left to acclimatize for 16–18 h in the dark. Overlying water was carefully added to each sediment core preventing resuspension and was continuously homogenized with a central stirring mechanism attached to the lid of each core which functioned during the entire incubation. Intertidal incubations used overlying unfiltered water pumped directly from the Eastern Scheldt at the institute which is located in relatively close proximity to the intertidal sites. The water collected at subtidal sampling stations was used as overlying unfiltered water for subtidal samples. In ideal circumstances, representative water directly from intertidal sample sites would have been collected, however, logistic time-constraints prevented this from happening.

Upon the addition of overlying water, aeration was stopped, a T_0 water sample was taken, and the cores were sealed airtight and dark O_2 incubations were started. Optode sensors (FireStingO2, Pyroscience) were used to measure oxygen concentrations in the overlying water at an interval of 30 s during the incubation period. After 4 h, the cores were opened and re-aerated for ensuing nutrient flux incubations in the dark. Water samples were collected at 4, 8, and 22 h after the start of the incubation period (after the T_0 water sample), filtered (0.45 μm; GF/F Whatman) into 6 ml polystyrene vials, and frozen (−20 C°) for nutrient analysis. Determination of nutrients followed the same procedure used for porewater nutrient samples.

All flux calculations across the sediment-water interface were obtained by fitting a linear regression on the concentration changes over time and multiplying the regression coefficient with the height of the overlying water column. A positive flux denotes an efflux or release from the sediment to the water column, and a negative flux an influx, or consumption of the solute by the sediment.

Organic matter mineralization was calculated assuming a molar ratio 1:1 carbon (C) to O_2 fluxes. Phosphorus (P) and nitrogen (N) mineralization were calculated from Redfield ratios 106:1 (C:P) and 106:16 (C:DIN), respectively.

$$DIN\ remineralization = O_2\ Flux * \frac{16}{106}$$

$$P\ remineralization = O_2\ Flux * \frac{1}{106}$$

The percentage of mineralized N and P removed from the system was calculated with the following equations:

$$DIN\ removed = \left(1 - \frac{DIN\ Flux}{DIN\ remineralization}\right) * 100$$

$$P\ removed = \left(1 - \frac{PO_4^{3-}\ Flux}{P\ remineralization}\right) * 100$$

Values over 100% imply an influx of solutes into sediment, so that nutrient removal is higher than the nutrients generated by mineralization. The nutrients removed in addition to those mineralized are taken up from the water column.

2.6. Statistical analysis

All statistical analyses for this study were performed using R (R Core Team, 2020). To assess statistically significant differences between intertidal and subtidal samples, generalized linear mixed models (GLMM) were used (Bolker et al., 2009) using 'zone' (intertidal or subtidal) and 'temperature' as fixed effects and 'station' and 'replicate' as random effect variables. GLMM's were created using the *glmer*-function in the R package "lme4" (Bates et al., 2015). For each parameter a full model (fixed and random effect variables) was run against a reduced model with only random effects using a partial F-Test. The residual error structure of the response variables featured gamma distributions which was incorporated in the GLMM's. A log link function was specified to account for non-linearity between predictor and mean response variables. Additional information on the statistical models used can be found in Table 1. Water column concentrations (2016–2017) and sediment type distribution in the ES (2016) was obtained from Rijkswaterstaat (Rijkswaterstaat, 2016, n.d.). Geospatial analysis was done with the program QGIS (QGIS Development Team, 2021).

3. Results

3.1. Environmental conditions and dry sediment parameters

Water temperature ranged from 7.1 to 9.9 °C in the winter to 16.9–19.7 °C in the summer months (**Supplementary** Figure B 1 to Figure B 6). Mean organic carbon stocks from intertidal stations OP (sandy) and DT (sandy), and ZK (muddy), accounted for 0.55, 0.10 and 0.79 kg C m^{-2} (equivalent to 46.1, 8.1 and 66.2 mol m^{-2}) in the upper 10 cm of the sediment, respectively. Organic carbon stocks for subtidal HM (sandy), VN (muddy) and LG (sandy) measured 0.23, 0.98, and 0.93 kg m^{-2} (19.6, 82.0 and 77.5 mol m^{-2}), respectively.

On average, intertidal stations displayed lower OC percentages and higher chl a concentration compared to subtidal sites (Table 2). Muddy stations (ZK/VN) had the highest concentrations of OC, TN, and phytopigments (chl a, pheophorbide, phaeophytin), while their OM reactivity scores (chl a/[chl a + Phaeophytin]), were lower than those of sandy stations within their respective zones (Table 2). Overall, OM reactivity was significantly higher (19%) in the intertidal compared to the subtidal samples ($p < 0.05$). Details for seasonal chl a concentration in the intertidal/subtidal and macrofauna assemblages are documented in De Borger et al. (2020). Solid-P and solid-Fe were highest, on average, in the muddy stations but showed high variability for all stations except for DT, which displayed the lowest solid-P and solid-Fe values in the study (Table 2).

3.2. Sediment-water exchange fluxes

Solute fluxes (O_2, NH_4^+, NO_2^-, NO_3^-, PO_4^{3-} and DSi) were seasonally variable with an increase in fluxes in warmer months (Fig. 2; **Supplementary Figure B 1**–Figure **B 6**). Maximum O_2 influxes (fluxes directed into the sediment) in the intertidal incubations were observed in August 2017 (−78.8 mmol m^{-2} d^{-1}) while maximum O_2 influxes in the subtidal incubations occurred in August 2016 (−63.9 mmol m^{-2} d^{-1}; Fig. 2). The maximum for ammonium effluxes (fluxes directed out of the sediment) was observed in the subtidal incubations in August 2016 at 4.0 mmol m^{-2} d^{-1} while maximum values for NH_4^+ effluxes in the intertidal samples were observed in September 2016 at 5.5 mmol m^{-2} d^{-1}. Nitrate fluxes in intertidal samples were almost always directed into the sediment with the highest mean influxes occurring in September 2016 (−3.2 mmol m^{-2} d^{-1}). Subtidal NO_3^- displayed effluxes with a maximum of 0.79 mmol m^{-2} d^{-1} in November 2017. Phosphate fluxes in intertidal and subtidal samples fluctuated within 0.6 and −0.4 mmol m^{-2} d^{-1} displaying an average influx for intertidal incubations throughout most of the sampling period apart from the warmer months (June–October) of 2017, while effluxes from subtidal samples were higher in the summer months for both years. Mean DSi effluxes were highest in subtidal samples reaching a maximum in July 2016 at 7.1 mmol m^{-2} d^{-1} (Fig. 2).

Mean O_2 ($p < 0.001$), PO_4^{3-} ($p < 0.001$) and NO_3^- ($p < 0.01$), had significantly greater influxes in the intertidal samples and the latter two solutes showed an efflux in subtidal stations (Fig. 2, Table 3). Subtidal stations displayed significantly higher total DIN, and DSi effluxes compared to intertidal stations ($p < 0.001$). Details for temporal fluxes at individual stations can be found in Supplementary **Figure B 1** and **Figure B 6**.

Intertidal sediments in ZK, DT and OP mineralized 21.1, 16.6 and 10.8 mol C m^{-2} y^{-1} compared to 14.0, 13.4 and 8.1 mol C m^{-2} y^{-1} at subtidal sites LG, HM, and VN, respectively. ZK (muddy intertidal) exhibited the strongest fluxes of O_2, NH_4^+, NO_3^-, and DSi. The muddy

Table 1
Results from Generalized Linear Mixed Effects Models (GLMM) used to test differences between intertidal and subtidal samples. For each parameter a full model containing fixed and random effects was run against a reduced model which contained only random effects using a partial F-Test. Fixed effects included 'Zone' (intertidal or subtidal) and 'Temperature'. Random effects included 'Station' (sampling location) and 'Replicate'.

Models		
Full model: Parameter ~ Zone + Temperature + Ɛ (Station) + Ɛ (Replicate)		
Reduced model: Parameter ~ Ɛ (Station) + Ɛ (Replicate)		
Parameter	**χ^2 (df = 2)**	***p* – value**
Dry sediment parameters		
Median grain size (um)	0.680	0.712
OC (%)	0.916	0.632
TN (%)	1.97	0.373
chl a	4.67	0.0965
Phaeophorbide	4.86	0.088
Phaeophytin	2.05	0.358
OM reactivity score (chl a/[chl a + Phaeophytin])	9.03	**p ≤ 0.05**
Biogeochemical Fluxes		
O_2 flux	44.2	**p ≤ 0.05**
NH_4^+	64.1	**p ≤ 0.05**
NO_2^-	6.05	**p ≤ 0.05**
NO_3^-	13.8	**p ≤ 0.05**
PO_4^{3-}	29.1	**p ≤ 0.05**
DSi	79.3	**p ≤ 0.05**
DIN flux	52.9	**p ≤ 0.05**
Nutrient removal		
Nitrogen removal	37.3	**p ≤ 0.05**
Phosphorus removal	41.4	**p ≤ 0.05**
% Nitrogen removal	27.8	**p ≤ 0.05**
% Phosphorus removal	18.1	**p ≤ 0.05**
Porewater Nutrients		
NH_4^+	10.2	**p ≤ 0.05**
NO_2^-	4.11	0.128
NO_3^-	14.5	**p ≤ 0.05**
PO_4^{3-}	1.57	0.456
DSi	5.12	0.077
DIN	11.5	**p ≤ 0.05**

Table 2
Dry sediment parameters for Eastern Scheldt stations: median grain size (D50; μm), porosity, organic carbon (OC; %) and total nitrogen (TN; %), chlorophyll *a* (chl a; μg g^{-1}), phaeophorbide (μg g^{-1}), phaeophytin (μg g^{-1}), OM reactivity score (chl a/(chl a + Phaeophytin)), solid phase phosphorus (solid-P; mol m^{-3} bulk solid) and iron (solid-Fe; mol m^{-3} bulk solid). Measurements were averaged for samples taken within 0 and 5 cm depths in the sediment. Significant figures are reported differently in accordance to the parameter.

	ZK	OP	DT	Combined Intertidal	VN	LG	HM	Combined Subtidal
D50[a]	56.0 ± 16.4	124 ± 10.8	139 ± 1.92	106 ± 38.6	65.3 ± 71.6	117 ± 8.3	195 ± 45.3	126 ± 72.0
Porosity[a]	0.52 ± 0.08	0.46 ± 0.12	0.40 ± 0.09	0.46 ± 0.10	0.60 ± 0.06	0.42 ± 0.05	0.34 ± 0.05	0.46 ± 0.12
OC[a]	0.83 ± 0.40	0.17 ± 0.04	0.06 ± 0.01	0.34 ± 0.41	1.1 ± 0.42	0.56 ± 0.14	0.37 ± 0.07	0.67 ± 0.39
TN	0.10 ± 0.04	0.02 ± 0.002	0.01 ± 0.002	0.04 ± 0.05	0.13 ± 0.06	0.05 ± 0.01	0.04 ± 0.01	0.07 ± 0.05
chl a[a]	22 ± 3.5	11 ± 2.7	9.3 ± 2.5	14 ± 6.4	13 ± 6.7	6.1 ± 4.2	5.8 ± 4.5	8.4 ± 6.3
phaeophorbide	1.0 ± 0.73	0.48 ± 0.38	0.07 ± 0.08	0.53 ± 0.62	3.4 ± 2.0	0.89 ± 0.78	1.7 ± 1.9	2.0 ± 1.9
phaeophytin	3.3 ± 1.6	1.1 ± 2.3	0.31 ± 0.25	1.6 ± 2.0	5.3 ± 3.7	1.6 ± 1.4	1.5 ± 1.4	2.8 ± 3.0
OM reactivity	0.88 ± 0.04	0.92 ± 0.07	0.97 ± 0.01	0.92 ± 0.06	0.70 ± 0.10	0.80 ± 0.08	0.81 ± 0.07	0.77 ± 0.09
solid-P	8.6 ± 9.2	3.0 ± 3.2	1.7 ± 1.9	4.5 ± 6.3	8.0 ± 10.6	5.0 ± 6.1	3.2 ± 3.6	5.4 ± 7.3
solid-Fe	145 ± 156	47.9 ± 51.3	28.4 ± 30.4	73.7 ± 106	149 ± 187	73.8 ± 79.0	92.5 ± 117	105 ± 133

[a] Recalculated from De Borger et al. (2020) with additional data.

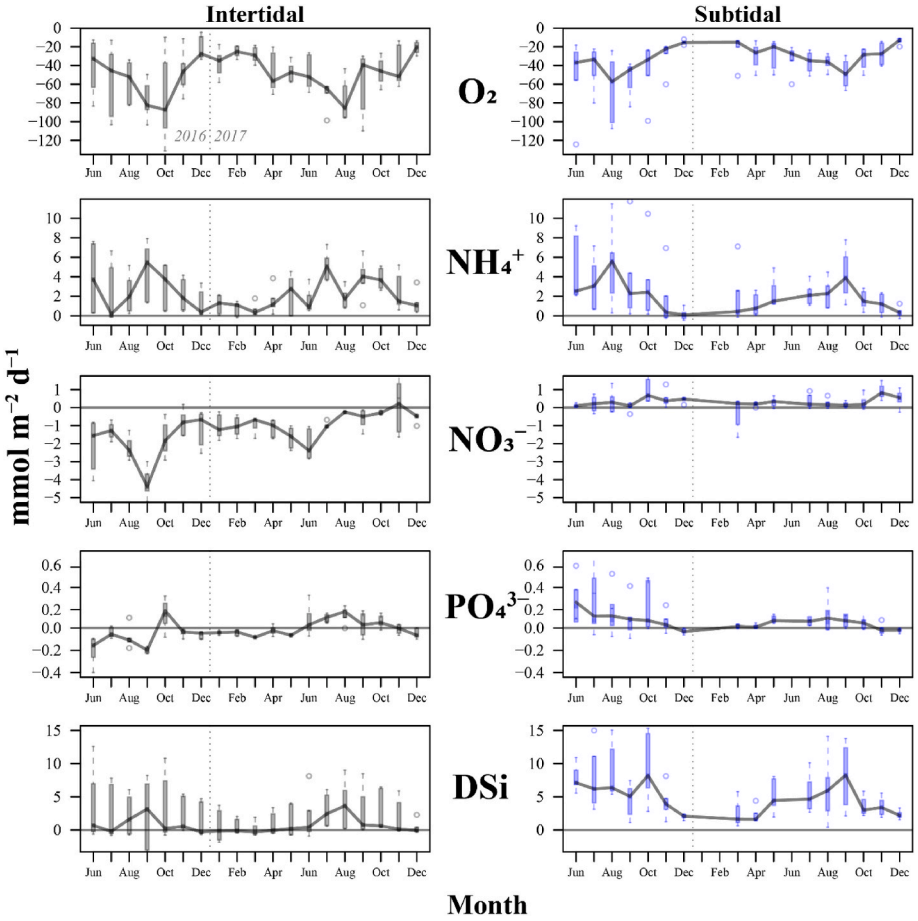

Fig. 2. Temporal comparison of sediment water exchange fluxes for oxygen and inorganic nutrient between subtidal and intertidal stations. The dark line represents the monthly median flux value with boxplots representing the monthly distribution of the data (minimum/maximum, interquartile range). Negative values denote an influx from the overlying water directed into the sediment.

subtidal site VN displayed the weakest fluxes for O_2 and NH_4^+ (Table 3). Intertidal sediments had higher macrofaunal abundance but lower biomass than subtidal sites (De Borger et al., 2020).

Measured nutrient fluxes deviated considerably from the fluxes based on OC mineralization, and assuming Redfield stoichiometric ratios. C:DIN flux ratios from intertidal samples were, on average, higher but more variable than those from the subtidal stations (Fig. 3). In intertidal samples, the deviations from Redfield were lowest for station OP and highest for station DT. On average the DIN:DIP ratio of fluxes exceeded Redfield (16:1), indicating that phosphorus was more efficiently removed than nitrogen for most stations (Fig. 3).

3.3. Porewater nutrients

In contrast to nutrient fluxes, porewater nutrients did not show noticeable levels of seasonality in either zone and were therefore pooled for further analysis. Mean porewater concentrations (0–10 cm depth) of NH_4^+ ($p < 0.01$) were significantly higher in subtidal (299 ± 209 mmol m^{-3}) compared to intertidal (83.4 ± 45.4 mmol m^{-3}) stations. NO_3^- concentrations were higher in the intertidal (5.1 ± 5.7 mmol m^{-3}) than

Table 3
Annually averaged mean (± standard deviation) daily sediment-water exchange fluxes for oxygen, ammonium, nitrite, nitrate, phosphate, silica, calculated nitrogen (N) and phosphorus (P) mineralization, and the calculated removal of N and P (all units in: mmol m^{-2} d^{-1}). Negative fluxes indicate sediment influx and positive are sediment effluxes. Significant figures are reported differently in accordance to the parameter.

	ZK	OP	DT	Combined Intertidal	VN	LG	HM	Combined Subtidal
O_2	−59.7 ± 23.2	−30.3 ± 14.8	−48.9 ± 18.1	−46.3 ± 22.4	−24.7 ± 9.7	−40.2 ± 19.6	−36.7 ± 18.6	−33.9 ± 17.6
NH_4^+	3.5 ± 1.7	1.9 ± 1.6	1.0 ± 1.2	2.1 ± 1.8	1.1 ± 0.91	3.3 ± 2.3	2.7 ± 2.7	2.4 ± 2.3
NO_2^-	0.16 ± 0.08	0.05 ± 0.07	0.12 ± 0.21	0.11 ± 0.15	0.19 ± 0.21	0.26 ± 0.19	0.13 ± 0.17	0.19 ± 0.19
NO_3^-	−1.8 ± 0.55	−0.99 ± 0.62	−0.96 ± 0.84	−1.24 ± 0.77	0.48 ± 0.38	0.14 ± 0.56	0.24 ± 0.28	0.28 ± 0.44
PO_4^{3-}	0.001 ± 0.06	−0.04 ± 0.07	−0.04 ± 0.06	−0.03 ± 0.07	0.06 ± 0.07	0.07 ± 0.10	0.13 ± 0.22	0.09 ± 0.14
DSi	4.5 ± 2.2	0.72 ± 1.5	−0.53 ± 0.56	1.6 ± 2.6	4.5 ± 2.4	5.5 ± 2.8	5.2 ± 4.0	5.1 ± 3.1
N mineralized	9.0 ± 3.5	4.6 ± 2.2	7.4 ± 2.7	6.7 ± 3.8	3.7 ± 1.5	6.1 ± 3.0	5.5 ± 2.8	5.1 ± 2.7
P mineralized	0.56 ± 0.21	0.29 ± 0.14	0.46 ± 0.16	0.44 ± 0.21	0.23 ± 0.08	0.38 ± 0.16	0.35 ± 0.23	0.32 ± 0.17
N removed	7.1 ± 2.7	3.6 ± 1.6	7.2 ± 2.4	6.0 ± 2.8	2.0 ± 0.89	2.3 ± 1.2	2.4 ± 1.1	2.3 ± 1.0
P removed	0.44 ± 0.17	0.23 ± 0.10	0.45 ± 0.15	0.37 ± 0.17	0.12 ± 0.05	0.15 ± 0.07	0.15 ± 0.07	0.14 ± 0.06
% N removed [a]	80.4 ± 13.7	82.7 ± 23.7	99.8 ± 14.6	87.7 ± 19.7	55.5 ± 16.9	42.6 ± 19.4	50.7 ± 21.0	49.6 ± 19.6
% P removed [a]	103 ± 12.3	125 ± 33.3	111 ± 13.7	113 ± 23.5	77.5 ± 28.1	83.5 ± 22.2	74.6 ± 38.3	78.5 ± 30.0

[a] Values over 100% imply the that the sediment influx is higher than the nutrients generated by mineralization. The additional influx is taken up from the water column.

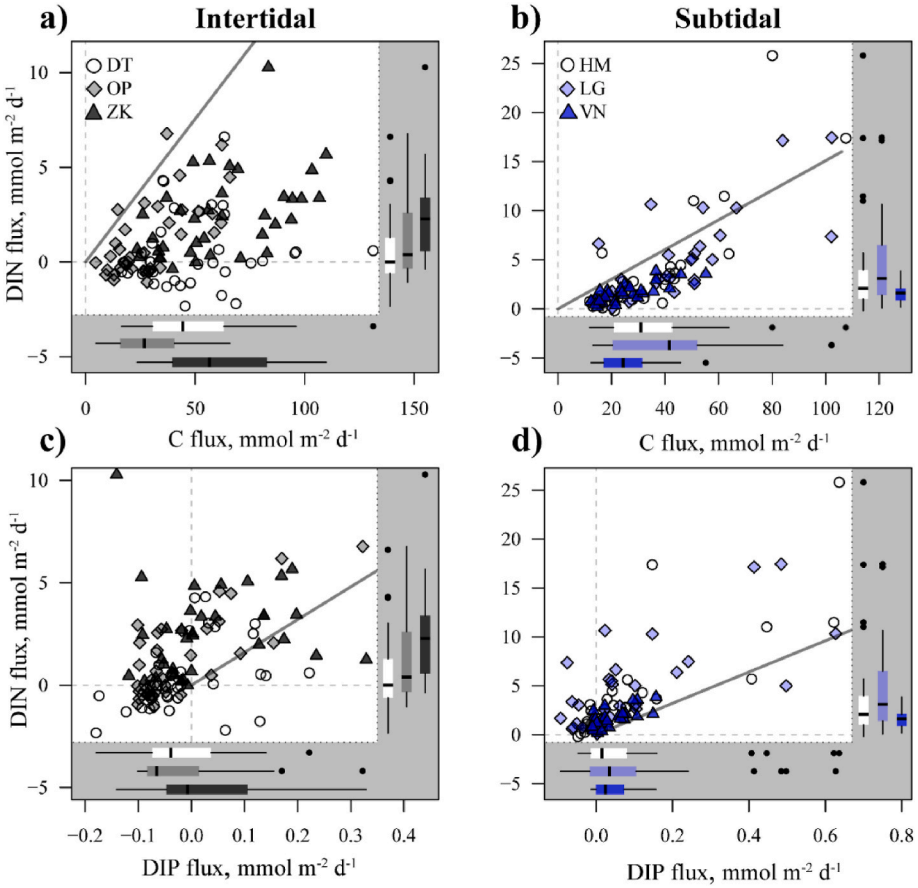

Fig. 3. Relation between dissolved inorganic nitrogen (DIN) and organic carbon (C) fluxes (a–b), DIN and dissolved inorganic phosphorus (DIP) fluxes (c–d). The dark line represents the Redfield (C:N:P = 106:16:1) ratio.

in subtidal (3.9 ± 3.7 mmol m^{-3}; $p < 0.001$) sediments. The highest concentrations of phosphate were found in the muddy stations of the intertidal (ZK; 86.4 ± 79.3 mmol m^{-3}) and subtidal (VN; 100 ± 35.6 mmol m^{-3}). VN also displayed the highest mean NH_4^+ (512 ± 172 mmol m^{-3}), and DSi (745 ± 162 mmol m^{-3}) concentrations (Fig. 4). The sandy intertidal DT station had the lowest concentration of DSi (23.8 ± 12.5 mmol m^{-3}), NH_4^+ (44.3 ± 22.8 mmol m^{-3}), and PO_4^{3-} (12.5 ± 8.3 mmol m^{-3}), but also exhibited the highest concentrations of NO_3^- (7.7 ± 6.9 mmol m^{-3}) mostly relegated to its upper (0–5 cm depth) sediment layers (Fig. 4). Sediment porewater contained more phosphorus than expected from the N:P Redfield ratio (16:1; Fig. 5). Data from the sandy intertidal and subtidal stations OP and HM, was the closest to the Redfield N:P proportion while other stations were skewed towards lower ratios. The DIN:DIP ratio of the sandy intertidal and subtidal stations was close to Redfield, while other stations were lower.

3.4. Nutrient removal

Nutrient removal refers to the processes through which inorganic nutrients released from mineralization become unavailable for primary production. This may occur, for example, through denitrification (bioavailable nitrogen converted to gaseous nitrogen), burial or

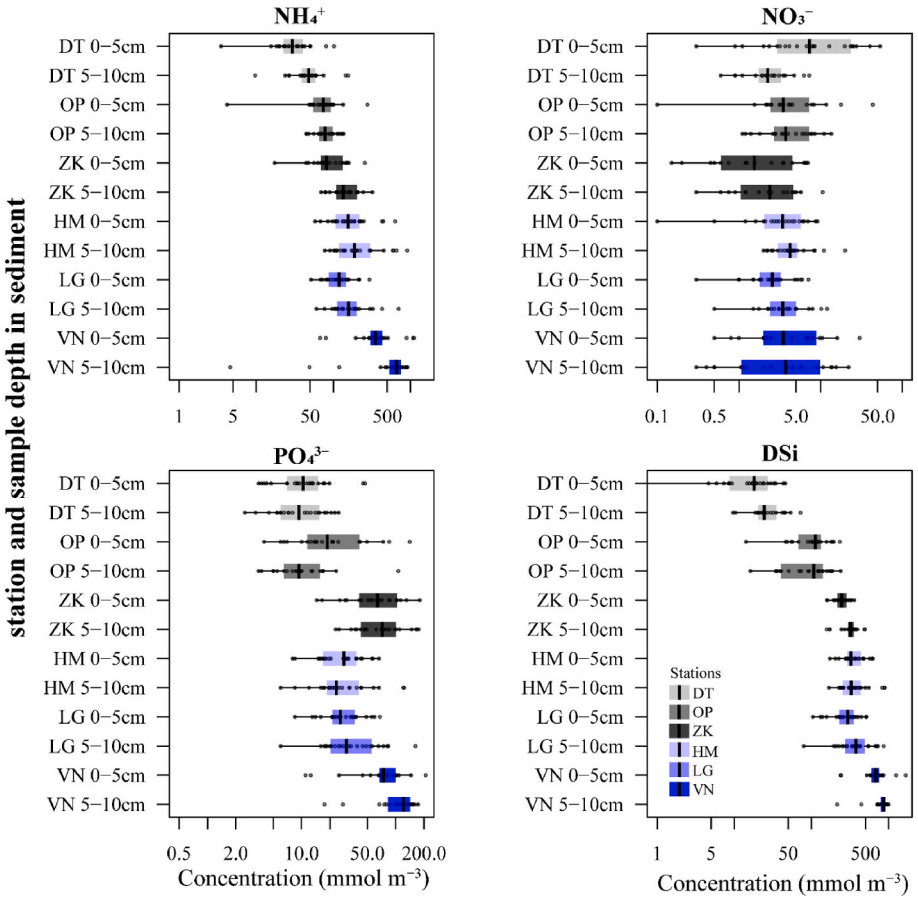

Fig. 4. Porewater nutrient concentrations shown in logarithmic scale for ammonium (NH_4^+) nitrate (NO_3^-), phosphate (PO_4^{3-}) and dissolved silicate (DSi) in the top (0–5 cm) and bottom (5–10 cm) slices per station. Intertidal stations are shown in gray and subtidal in blue. Note differences in x-axis scale.

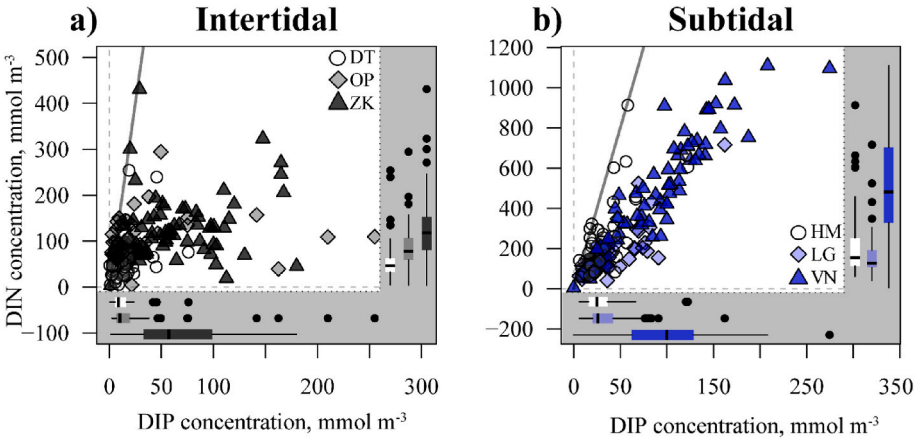

Fig. 5. The DIN:DIP relation in the sediment porewater (a and b) in subtidal and intertidal stations. The dark line represents the expected Redfield (C:N:P = 106:16:1) ratio.

sediment sorption (bioavailable nutrients which are isolated within the sediment). Combined incubations from intertidal stations removed a significantly higher percentage of total inorganic nitrogen (N) and phosphorus (P) (87.7% and 113%, respectively) after mineralization ($p < 0.001$) compared to combined incubations from subtidal stations (49.6% and 78.5%, respectively; Table 3). The percentage of inorganic N or P removed during incubations from intertidal sediments regularly exceeded 100%. This indicates that nutrient removal was higher than nutrient release from mineralization and thus additional solutes from the overlying water were utilized. Over the 1.5 year monitoring period, a nutrient removal rate exceeding 100% for N and P was observed in 31% and 75% of incubations from intertidal sites, while in subtidal sites N removal was never observed and P removal occurred in 18% of the incubations.

In subtidal incubations, percentage P removal was highest in the sandy LG station. In intertidal sediments, the observed percentage N removal capacity was highest at the sandy site DT (Table 3). Bioavailable phosphorus was preferentially trapped in intertidal sediments where over 100% of P was removed after mineralization. The total N and P removal per meter squared was also significantly higher in the

intertidal compared to the subtidal ($p < 0.001$) with the highest values for N and P removal coming from DT in the intertidal and the lowest values exhibited in subtidal VN (Table 3).

4. Discussion

Our results reveal disparities in OM quality, sediment-water exchange fluxes, porewater solute concentrations and the nutrient removal capacity between specific intertidal and subtidal stations in the Eastern Scheldt. Overall, intertidal samples exhibited higher rates of OM cycling and nutrient removal compared to subtidal sediments. The conversion of intertidal to subtidal areas resulting from ongoing intertidal erosion may affect the biogeochemical dynamics of coastal areas and adjacent water bodies. Here we discuss the potential importance of each tidal zone for sedimentary carbon, the mechanisms behind ES nutrient dynamics, and end with an upscaling exercise to explore how future biogeochemical functioning may change based on the expected loss of intertidal surface area in the ES.

4.1. Carbon characteristics of Eastern Scheldt intertidal and subtidal areas

Our results suggest that microphytobenthos activity is a determining factor for carbon degradation and other biogeochemical dynamics. Intertidal sediments exhibit a higher chl a concentration and are characterized by high microphytobenthos densities (Serôdio and Paterson, 2021), compared to subtidal sediments. This is likely to be one of the factors contributing to the higher OM reactivity and enhanced rates of OM degradation (as inferred from measured O_2 fluxes) in intertidal compared to subtidal samples. Growth of microphytobenthos on ES intertidal flats may provide enough input of fresh OM to maintain a high reactivity score while fueling increased levels of carbon degradation. This pattern of more reactive OM in shallow vs deep marine habitats has also been found on continental shelf sediments surrounding the United Kingdom and France (Lamarque et al., 2021; Smeaton and Austin, 2022). Reduced DSi concentrations found in intertidal (vs. subtidal) porewater samples (Fig. 4) provide further evidence of diatom (microphytobenthos) uptake of DSi.

De Borger et al. (2020) describes the relationship between macrobenthos and bioirrigation in the Eastern Scheldt and combined with results from the current study can give valuable insight on how ES fauna affects carbon cycling. ES intertidal sites are associated with prominent bioirrigators with DT being dominated by burrowing amphipods (*Corophium* sp., *Bathyporeia* sp.) while OP and ZK assemblages are linked with the large polychaetes *Arenicola marina* and *Hediste diversicolor* (De Borger et al., 2020). In contrast, subtidal ES sites are associated with epifaunal assemblages (species residing on the sediment surface) except for LG where the tube building polychaete *Lanice conchilega* is commonly found in the cooler months of the year (De Borger et al., 2020). Our results of higher O_2 consumption (and estimated carbon mineralization) from ES intertidal samples (Table 3) are consistent with De Borger et al. (2020)'s observations of 'deeper' bioirrigation in ES intertidal versus subtidal sediments. This suggests that ES faunal assemblages that cause solute exchange within deeper portions of the sediment, such as those found in the intertidal sites, may facilitate higher rates of organic carbon mineralization (De Borger et al., 2020).

Temperate coastal environments in other parts of the world display higher percentages of organic carbon compared to the ES (Byun et al., 2019; Douglas et al., 2022; Falcão and Vale, 1998). This difference could be related to the reduced input of sedimentary OM to the ES due to the almost absent riverine input; and to the net export of sediments and sedimentary OM to the North Sea created after flood mitigation developments (Jiang et al., 2020; van Zanten and Adriaanse, 2008; Wetsteyn et al., 2003). The construction of the storm surge barrier in the ES has also reduced water column nutrient concentrations by limiting riverine input (Smaal and Nienhuis, 1992). Understanding the tight coupling between OM production and inorganic nutrients in the ES involves knowledge of biogeochemical processes affecting nutrient availability.

4.2. Nutrient dynamics and removal in the Eastern Scheldt

Inorganic nutrient concentrations in porewater, sediment-water exchange fluxes, and benthic removal processes (the long-term sequestration of bioavailable nutrients) depend on abiotic variables such as sediment type (Precht et al., 2004) and biotic variables including the presence of microphytobenthos and/or benthic faunal activity (de Backer et al., 2010; De Borger et al., 2020). Our study highlights fundamental disparities in nutrient removal functions between subtidal and intertidal sediments, which were detected upon the analysis of porewater nutrients and the exchange fluxes of NO_3^- and PO_4^{3-}.

Coarse sediments promote nitrification, nutrient release and porewater advection (Precht et al., 2004), and typically exhibit low concentrations of porewater nutrients (De Borger et al., 2021). Muddy ES sediments (ZK and VN) indeed hold higher NH_4^+ and PO_4^{3-} concentrations (Fig. 4), compared to adjacent sandy sites, a pattern consistent with other temperate sedimentary systems (Berthold et al., 2018; Falcão and Vale, 1998). Small sediment particles exhibit an increased PO_4^{3-} sorption capacity compared to bigger sand particles (Borggaard, 1983). Moreover, muddy sediments have a lower oxygen content which facilitates the desorption of PO_4^{3-} from iron oxides at depth promoting the release of bioavailable phosphorus in porewater (Slomp et al., 1996). This eventually translates in higher concentrations of PO_4^{3-} at depth, like those observed in ZK and VN.

Subtidal sediments displayed relatively high porewater concentrations of NH_4^+, PO_4^{3-} and DSi, possibly resulting from the lower levels of bioirrigation which have been found at these sites (De Borger et al., 2020). Bioirrigation can increase the oxygenation of sediments and can indirectly enhance nutrient removal processes such as denitrification (Braeckman et al., 2010, 2014). Less bioirrigation leads to lower removal and flushing of nutrients causing their accumulation in porewaters and subsequent release to the water column by diffusion, as suggested by the prevalent efflux NH_4^+, PO_4^{3-} and DSi (Fig. 2) in the subtidal samples.

A higher chl a concentration in intertidal sites (Table 2) suggested that microphytobenthic OM helps fuel the rapid mineralization measured in those sites (Table 3), and may potentially support denser benthic communities (De Borger et al., 2020) than in the subtidal sites. The relatively low concentrations of OC, TN (Table 2), NH_4^+, DSi and PO_4^{3-}, and higher NO_3^- (Fig. 4) observed in intertidal sites porewater may result from higher mineralization, bioirrigation (de Backer et al., 2010; De Borger et al., 2020), tidal flushing (Falcão and Vale, 1998) and/or porewater advection (Precht et al., 2004). These factors facilitate processes that decrease porewater solutes such as nitrification-denitrification, nutrient flushing, and the sorption of phosphates. Influxes of NO_3^- and PO_4^{3-} (as opposed to effluxes; Fig. 2) observed in the intertidal incubations suggest enhanced sorption of phosphate to sediment particles and higher denitrification than in the subtidal samples; results in agreement with other studies (Piehler and Smyth, 2011). Furthermore, intertidal samples removed on average 80% of mineralized dissolved inorganic nitrogen (DIN) and at least 100% of mineralized dissolved inorganic phosphorus (DIP) (Table 3). Intertidal nutrient influxes have been observed in other coastal systems (Khalil et al., 2018; Magalhães et al., 2002) but they contrast with observations from the adjacent Western Scheldt estuary (Rios-Yunes et al., subm.) where an efflux of DIN and DIP was observed in brackish and marine intertidal mudflats.

The comparisons of the flux ratios with Redfield proportions (Fig. 3 a and 3 b) show the removal of bioavailable nitrogen, as the flux ratios of C:DIN exceed Redfield (C:N; 106:16). All ES sites also exhibited lower average DIN:DIP flux ratios compared to Redfield (N:P; 16:1) suggesting a proportionally greater sedimentary removal of P compared to N (Fig. 3

c and 3d, Table 3), similar to patterns observed in the Douro River estuary in Portugal (Magalhães et al., 2002). While nitrogen is lost from sediments as nitrogen gas, phosphorus is removed by burial in the sediment, often sorbed to solids. Moreover, the comparison between porewater concentration ratios with Redfield (Fig. 5 a and 5 b) evidenced the preferential removal of DIP over DIN of intertidal and subtidal sediments in this study. Particularly in the intertidal sediments, the DIN:DIP concentration ratio may strongly exceed Redfield (16:1), often leading to PO_4^{3-} concentrations that are as high as DIN (Fig. 5 a). Most of the burial of P is in solid form, as evidenced by the iron-bound phosphorus which measured over two orders of magnitude higher than porewater concentrations indicating high sorption of PO_4^{3-} in ES sediments (solid phase phosphorous in Table 2 in mol m^{-3}). By extrapolating information on nutrient removal to total surface areas in the ES, we may be able to roughly predict the impact of future changes to the intertidal-subtidal dynamic.

4.3. Spatial analysis and future implications

Our study considers six sampling locations within the Eastern Scheldt tidal bay and we acknowledge that extrapolating from these stations may not lead to a completely accurate representation of biogeochemical dynamics within the system, particularly if certain important areas are underrepresented. Nevertheless, to gain a better understanding of how sediments may affect biogeochemical functioning in the ES, we conducted an upscaling exercise based on the assumption that the average parameters measured in the stations described in this study are representative of the greater ES system.

Our results were spatially interpolated to understand the overall contribution of each zone and sediment type to nutrient removal of the Eastern Scheldt system. The ES covers an area of 347 km^2 with 216 km^2 subtidal and 118 km^2 intertidal area. Of the intertidal area, 1.6 km^2 corresponds to muddy and ~117 km^2 to sandy sediments with the remaining area covered by a rocky bottom or saltmarshes. Yearly averaged system-wide mineralization budgets were calculated by considering the contribution of each sediment type to each tidal area. Currently, our estimates suggest that intertidal areas in the ES remove more nitrogen (2.3×10^8 mol N y^{-1}) than subtidal areas (1.8×10^8 mol N y^{-1}), but P removal seems to be similar between these zones (both with ~1.8×10^7 mol P y^{-1}). This means that if the ES was a closed system without external nutrient inputs, the average winter concentration of N and P in the water column (Rijkswaterstaat, n.d.) may be depleted in ~70 and 20 days, respectively. Assuming dynamic equilibrium for ES nutrient sources and sinks, this suggests a substantial input of nutrients from the North Sea to balance this removal. It is noteworthy that our calculation of nutrient removal may be conservative as it is based on dark respiration processes and no primary production has been considered. Primary production could increase nutrient removal through the biogenic uptake from microphytobenthos (Clavier et al., 2005).

A consequence of the flood mitigation developments in the ES has been the ongoing loss of intertidal areas due to “sand starvation”, and the reduced exchange of nutrients and OM with the North Sea (van Zanten and Adriaanse, 2008; Wetsteyn et al., 2003). It is estimated that erosion will contribute to a 35% loss of intertidal areas in the next four decades (Ysebaert et al., 2016). Following Ysebaert et al. (2016)’s estimates, eroding intertidal areas will increase the ES subtidal area by 19% potentially reducing the total sedimentary (subtidal + intertidal) nutrient removal of the ES. If the measurements from this study are representative of the greater ES region and if they remain consistent over time, we calculate an erosion induced decrease in the total nitrogen removal capacity from 4.1×10^8 mol N y^{-1} to 3.7×10^8 mol N y^{-1} (11%). We also expect that the future removal capacity of phosphorus to decrease from 3.6×10^7 mol P y^{-1} to 3.3×10^7 mol P y^{-1} (8%). The loss of intertidal surface area could compromise areas important for OM mineralization and nutrient cycling and may decrease important ecosystem functions such as nitrogen/phosphorus removal, potentially increasing the concentration of nutrients available for primary production.

Sea level rise (SLR) presents an additional threat to ES intertidal areas (Fox-Kemper et al., 2021). Estimates for SLR in the North Sea close to the ES predict an increase of ~17.1 cm following the SSP1-1.9 (Paris) scenario and 27.8 cm for the SSP5-8.5 by 2060 (pers. Comm. Aimée Slangen, (Fox-Kemper et al., 2021). The inclusion of SLR estimates for coastal systems is highly complex and is still in its infancy. A study on future SLR in the ES concluded that tidal amplitude would increase, and that the ES would become ebb-dominated (Jiang et al., 2020). A transition to ebb-dominance in an already sand-starved system like the ES means that erosion of the intertidal zone, and the resulting loss of nutrient removal capacity would be exacerbated in the future.

It is noteworthy that the future estimates we present may be conservative as they do not account for SLR and might be underestimating the potential loss of nutrient removal capacity in the ES. This can be concerning for a system like the ES due to its ecological and cultural importance. Alterations to its biogeochemical regime, nutrients and primary production can affect the local and migratory species and have consequences for economic activities (Nienhuis and Smaal, 1994; Ysebaert et al., 2016; Zwarts et al., n.d.). Studying how SLR and sand starvation could affect intertidal areas and corresponding nutrient removal functions in coastal areas is therefore important to understand future biogeochemical characteristics of these areas.

To conclude, our study shows that the mineralization and bioavailable removal of inorganic nutrients can be significantly higher in intertidal sediments than in subtidal areas. These results are highly relevant since intertidal areas around the world are receding due to coastal development, erosion, and sea-level rise (Murray et al., 2019). Mudflats cover ~127,000 km^2 worldwide, and their decline may have consequences on local and regional biogeochemical functioning. Therefore, improved understanding of tidal flat ecosystems is essential to manage and/or mitigate potential reductions to their functions and services. In addition, the relevance of investigating the Dutch coastal zone is that it is one of the most extensively engineered areas in the world. Thus, the environmental consequences derived from the loss of intertidal areas in Dutch systems could serve as a case study to guide future coastal protection projects elsewhere, and to some extent, prevent undesirable environmental problems derived from extensive coastal engineering, coastal erosion, and rising sea levels.

Declaration of competing interest

The authors declare the following financial interests/personal relationships which may be considered as potential competing interests: Dunia Rios-Yunes reports financial support was provided by Royal Netherlands Academy of Arts and Sciences. Justin C. Tiano reports financial support was provided by Ministry of Agriculture Nature and Food Quality. Justin C. Tiano reports financial support was provided by European Maritime and Fisheries Fund.

Acknowledgements

We thank Rijkswaterstaat and the crew of their research vessel, the Delta, for making it possible to conduct the subtidal sampling for this study. We also thank various students who have helped with collecting and processing the information for this study. This work could not have been done without the help of the NIOZ analytical lab (Peter van Breugel, Yvonne Maas, Jan Peene, Jurian Brasser and more) which processed our sediment and water samples. Dunia Rios Yunes is a doctoral research fellow funded by the Royal Netherlands Academy of Arts and Sciences (KNAW) (project no. PSA-SA-E-02). Justin Tiano was supported by the Netherlands Ministry of Agriculture, Nature and Food Quality (LNV) and European Maritime and Fisheries Fund (EMFF) (grant no. 1300021172).

Appendix A. Supplementary data

Supplementary data to this article can be found online at https://doi.org/10.1016/j.csr.2022.104904.

References

Arndt, S., Jørgensen, B.B., LaRowe, D.E., Middelburg, J.J., Pancost, R.D., Regnier, P., 2013. Quantifying the degradation of organic matter in marine sediments: a review and synthesis. Earth Sci. Rev. 123, 53–86. https://doi.org/10.1016/j.earscirev.2013.02.008.

Bates, D., Mächler, M., Bolker, B., Walker, S., 2015. Fitting linear mixed-effects models using lme4. J. Stat. Software 67. https://doi.org/10.18637/jss.v067.i01.

Berthold, M., Zimmer, D., Reiff, V., Schumann, R., 2018. Phosphorus contents Re-visited after 40 Years in muddy and sandy sediments of a temperate lagoon system. Front. Mar. Sci. 5 https://doi.org/10.3389/fmars.2018.00305.

Bolker, B.M., Brooks, M.E., Clark, C.J., Geange, S.W., Poulsen, J.R., Stevens, M.H.H., White, J.-S.S., 2009. Generalized linear mixed models: a practical guide for ecology and evolution. Trends Ecol. Evol. 24, 127–135. https://doi.org/10.1016/j.tree.2008.10.008.

Bonifácio, P., Bourgeois, S., Labrune, C., Amouroux, J.M., Escoubeyrou, K., Buscail, R., Romero-Ramirez, A., Lantoine, F., Vétion, G., Bichon, S., Desmalades, M., Rivière, B., Deflandre, B., Grémare, A., 2014. Spatiotemporal changes in surface sediment characteristics and benthic macrofauna composition off the Rhône River in relation to its hydrological regime. Estuar. Coast Shelf Sci. 151, 196–209. https://doi.org/10.1016/j.ecss.2014.10.011.

Borggaard, O.K., 1983. Effect of surface area and mineralogy of iron oxides on their surface charge and Anion-adsorption properties. Clay Clay Miner. 31, 230–232. https://doi.org/10.1346/CCMN.1983.0310309.

Braeckman, U., Provoost, P., Gribsholt, B., van Gansbeke, D., Middelburg, J., Soetaert, K., Vincx, M., Vanaverbeke, J., 2010. Role of macrofauna functional traits and density in biogeochemical fluxes and bioturbation. Mar. Ecol. Prog. Ser. 399, 173–186. https://doi.org/10.3354/meps08336.

Braeckman, U., van Colen, C., Guilini, K., van Gansbeke, D., Soetaert, K., Vincx, M., Vanaverbeke, J., 2014. Empirical evidence reveals seasonally dependent reduction in nitrification in coastal sediments subjected to near future ocean acidification. PLoS One 9. https://doi.org/10.1371/journal.pone.0108153.

Bulmer, R.H., Stephenson, F., Jones, H.F.E., Townsend, M., Hillman, J.R., Schwendenmann, L., Lundquist, C.J., 2020. Blue carbon stocks and cross-habitat subsidies. Front. Mar. Sci. 7 https://doi.org/10.3389/fmars.2020.00380.

Byun, C., Lee, S.H., Kang, H., 2019. Estimation of carbon storage in coastal wetlands and comparison of different management schemes in South Korea. J Ecol Environ 43. https://doi.org/10.1186/s41610-019-0106-7.

Cabrita, M.T., Catarino, F., Vale, C., 1999. The effect of tidal range on the flushing of ammonium from intertidal sediments of the Tagus estuary, Portugal. Oceanol. Acta 22, 291–302. https://doi.org/10.1016/S0399-1784(99)80053-X.

Clavier, J., Boucher, G., Chauvaud, L., Fichez, R., Chifflet, S., 2005. Benthic response to ammonium pulses in a tropical lagoon: implications for coastal environmental processes. J. Exp. Mar. Biol. Ecol. 316, 231–241.

de Backer, A., van Ael, E., Vincx, M., Degraer, S., 2010. Behaviour and time allocation of the mud shrimp, Corophium volutator, during the tidal cycle: a laboratory study. Helgol. Mar. Res. 64, 63–67. https://doi.org/10.1007/s10152-009-0167-6.

De Borger, E., Braeckman, U., Soetaert, K., 2021. Rapid organic matter cycling in North Sea sediments. Continent. Shelf Res. 214, 104327 https://doi.org/10.1016/j.csr.2020.104327.

De Borger, E., Tiano, J., Braeckman, U., Ysebaert, T., Soetaert, K., 2020. Biological and biogeochemical methods for estimating bioirrigation: a case study in the Oosterschelde estuary. Biogeosciences 17, 1701–1715. https://doi.org/10.5194/bg-17-1701-2020.

Douglas, T.J., Schuerholz, G., Juniper, S.K., 2022. Blue carbon storage in a Northern temperate estuary subject to habitat loss and chronic habitat disturbance: Cowichan Estuary, British Columbia, Canada. Front. Mar. Sci. 9 https://doi.org/10.3389/fmars.2022.857586.

Eyre, B.D., Ferguson, A.J.P., Webb, A., Maher, D., Oakes, J.M., 2011. Denitrification, N-fixation and nitrogen and phosphorus fluxes in different benthic habitats and their contribution to the nitrogen and phosphorus budgets of a shallow oligotrophic sub-tropical coastal system (southern Moreton Bay, Australia). Biogeochemistry 102, 111–133. https://doi.org/10.1007/s10533-010-9425-6.

Falcão, M., Vale, C., 1998. Sediment—water exchanges of ammonium and phosphate in intertidal and subtidal areas of a mesotidal coastal lagoon (Ria Formosa). In: Oceans, Rivers and Lakes: Energy and Substance Transfers at Interfaces. Springer Netherlands, Dordrecht, pp. 193–201. https://doi.org/10.1007/978-94-011-5266-2_16.

Fox-Kemper, B., Hewitt, H.T., Xiao, C., Aðalgeirsdóttir, G., Drijfhout, S.S., Edwards, T.L., Golledge, N.R., Hemer, M., Kopp, R.E., Krinner, G., Mix, A., Notz, D., Nowicki, S., Nurhati, I.S., Ruiz, L., Sallée, J.-B., Slangen, A.B.A., Yu, Y., 2021. Ocean, cryosphere and sea level change. In: MassonDelmotte, V., Zhai, P., Pirani, A., Connors, S.L., Péan, C., Berger, S., Caud, N., Chen, Y., Goldfarb, L., Gomis, M.I., Huang, M., Leitzell, K., Lonnoy, E., Matthews, J.B.R., Maycock, T.K., Waterfield, T., Yelekçi, O., Yu, R., Zhou, B. (Eds.), Climate Change 2021: the Physical Science Basis. Contribution of Working Group I to the Sixth Assessment Report of the Intergovernmental Panel on Climate Change. Cambridge University Press.

Gilbert, A., Schaafsma, M., de Nocker, L., Liekens, I., Broekx, S., 2007. Case Study Status Report Scheldt River Basin, 10.1.1.713.9579.

Herbert, R., 1999. Nitrogen cycling in coastal marine ecosystems. FEMS Microbiol. Rev. 23, 563–590. https://doi.org/10.1016/S0168-6445(99)00022-4.

Hilmi, N., Chami, R., Sutherland, M.D., Hall-Spencer, J.M., Lebleu, L., Benitez, M.B., Levin, L.A., 2021. The role of blue carbon in climate change mitigation and carbon stock conservation. Front. Clim. 3 https://doi.org/10.3389/fclim.2021.710546.

IUCN, 2021. Blue Carbon [WWW Document]. URL. https://www.iucn.org/resources/issues-briefs/blue-carbon, 12.14.21.

Jiang, L., Gerkema, T., Idier, D., Slangen, A.B.A., Soetaert, K., 2020. Effects of sea-level rise on tides and sediment dynamics in a Dutch tidal bay. Ocean Sci. 16, 307–321. https://doi.org/10.5194/os-16-307-2020.

Jiang, L., Soetaert, K., Gerkema, T., 2019. Decomposing the intra-annual variability of flushing characteristics in a tidal bay along the North Sea. J. Sea Res. 155, 101821 https://doi.org/10.1016/j.seares.2019.101821.

Jodo, M., Kawamoto, K., Tochimoto, M., Coverly, S.C., 1992. Determination of nutrients in seawater by segmented–flow analysis with higher analysis rate and reduced interference on ammonia. J. Automat. Chem. 14, 163–167. https://doi.org/10.1155/S1463924692000300.

Joye, S.B., Paerl, H.W., 1993. Nitrogen fixation and denitrification in the intertidal and subtidal environments of Tomales Bay, California. In: Biogeochemistry of Global Change. Springer US, Boston, MA, pp. 633–653. https://doi.org/10.1007/978-1-4615-2812-8_35.

Kang, C.-K., Park, H.J., Choy, E.J., Choi, K.-S., Hwang, K., Kim, J.-B., 2015. Linking intertidal and subtidal Food webs: consumer-mediated transport of intertidal benthic microalgal carbon. PLoS One 10, e0139802. https://doi.org/10.1371/journal.pone.0139802.

Khalil, K., Laverman, A.M., Raimonet, M., Rabouille, C., 2018. Importance of nitrate reduction in benthic carbon mineralization in two eutrophic estuaries: modeling, observations and laboratory experiments. Mar. Chem. 199, 24–36. https://doi.org/10.1016/j.marchem.2018.01.004.

Khalil, K., Raimonet, M., Laverman, A.M., Yan, C., Andrieux-Loyer, F., Viollier, E., Deflandre, B., Ragueneau, O., Rabouille, C., 2013. Spatial and temporal variability of sediment organic matter recycling in two temperate Eutrophicated estuaries. Aquat. Geochem. 19, 517–542. https://doi.org/10.1007/s10498-013-9213-8.

Kristensen, E., Penha-Lopes, G., Delefosse, M., Valdemarsen, T., Quintana, C., Banta, G., 2012. What is bioturbation? The need for a precise definition for fauna in aquatic sciences. Mar. Ecol. Prog. Ser. 446, 285–302. https://doi.org/10.3354/meps09506.

Kuijper, K., Lescinski, J., 2013. Data-analysis water levels, bathymetry Western Scheldt. https://www.vnsc.eu/uploads/2014/02/g-5-data-analysis-water-levels-bathymetry-western-scheldt-v2-0.pdf.

Laffoley, D., Baxter, J.M., Thevenon, F., Oliver, J., 2014. The Significance and Management of Natural Carbon Stores in the Open Ocean. Gland, Switzerland.

Lamarque, B., Deflandre, B., Galindo Dalto, A., Schmidt, S., Romero-Ramirez, A., Garabetian, F., Dubosq, N., Diaz, M., Grasso, F., Sottolichio, A., Bernard, G., Gillet, H., Cordier, M.-A., Poirier, D., Lebleu, P., Derriennic, H., Danilo, M., Murilo Barboza Tenório, M., Grémare, A., 2021. Spatial distributions of surface sedimentary organics and sediment profile image characteristics in a high-energy temperate marine RiOMar: the west gironde mud patch. J. Mar. Sci. Eng. 9, 242. https://doi.org/10.3390/jmse9030242.

Laverock, B., Gilbert, J.A., Tait, K., Osborn, A.M., Widdicombe, S., 2011. Bioturbation: impact on the marine nitrogen cycle. Biochem. Soc. Trans. 39, 315–320. https://doi.org/10.1042/BST0390315.

Lessin, G., Artioli, Y., Almroth-Rosell, E., Blackford, J.C., Dale, A.W., Glud, R.N., Middelburg, J.J., Pastres, R., Queirós, A.M., Rabouille, C., Regnier, P., Soetaert, K., Solidoro, C., Stephens, N., Yakushev, E., 2018. Modelling marine sediment biogeochemistry: current knowledge gaps, challenges, and some methodological advice for advancement. Front. Mar. Sci. 5, 1–8. https://doi.org/10.3389/fmars.2018.00019.

Magalhães, C., Bordalo, A., Wiebe, W., 2002. Temporal and spatial patterns of intertidal sediment-water nutrient and oxygen fluxes in the Douro River estuary, Portugal. Mar. Ecol. Prog. Ser. 233, 55–71. https://doi.org/10.3354/meps233055.

Murray, N.J., Phinn, S.R., DeWitt, M., Ferrari, R., Johnston, R., Lyons, M.B., Clinton, N., Thau, D., Fuller, R.A., 2019. The global distribution and trajectory of tidal flats. Nature 565, 222–225. https://doi.org/10.1038/s41586-018-0805-8.

Nienhuis, P.H., Smaal, A.C., 1994. The Oosterschelde estuary, a case-study of a changing ecosystem: an introduction. In: The Oosterschelde Estuary (The Netherlands): A Case-Study of a Changing Ecosystem. Springer Netherlands, Dordrecht, pp. 1–14. https://doi.org/10.1007/978-94-011-1174-4_1.

Pastor, L., Deflandre, B., Viollier, E., Cathalot, C., Metzger, E., Rabouille, C., Escoubeyrou, K., Lloret, E., Pruski, A.M., Vétion, G., Desmalades, M., Buscail, R., Grémare, A., 2011. Influence of the organic matter composition on benthic oxygen demand in the Rhône River prodelta (NW Mediterranean Sea). Continent. Shelf Res. 31, 1008–1019. https://doi.org/10.1016/j.csr.2011.03.007.

Piehler, M.F., Smyth, A.R., 2011. Habitat-specific distinctions in estuarine denitrification affect both ecosystem function and services. Ecosphere 2. https://doi.org/10.1890/ES10-00082.1 art12.

Precht, E., Franke, U., Polerecky, L., Huettel, M., 2004. Oxygen dynamics in permeable sediments with wave-driven pore water exchange. Limnol. Oceanogr. 49, 693–705. https://doi.org/10.4319/lo.2004.49.3.0693.

QGIS Development Team, 2021. QGIS Geographic Information System.

R Core Team, 2020. R: A Language and Environment for Statistical Computing.

Riedl, R.J., Huang, N., Machan, R., 1972. The subtidal pump: a mechanism of interstitial water exchange by wave action. Mar. Biol. 13, 210–221. https://doi.org/10.1007/BF00391379.

Rijkswaterstaat, 2016. Ecotopenkaarten [WWW Document]. ecotopenkaart_oosterschelde_2016. URL. https://maps.rijkswaterstaat.nl/gwproj55/index.html?viewer=Ecotopen.Webviewer, 1.12.22.

n.d. Rijkswaterstaat, Rijkswaterstaat Waterinfo [WWW Document]. Nutriënten en eutrofiëringsparameters-OW. URL. https://waterinfo.rws.nl/, 8.2.22a.
n.d. Rijkswaterstaat, National Georegister [WWW Document]. URL. https://www.nationaalgeoregister.nl/geonetwork/srv//dut/catalog.search#/home, 10.15.21b.
Rios-Yunes, D., Tiano, J.C., van Oevelen, D., van Dalen, J., Soetaert, K., n.d. Annual Biogeochemical Cycling in Intertidal Sediments of a Restored Estuary Reveals Dependence of N, P, C and Si Cycles to Temperature and Water Column Properties. Submitted for publication.
Rocha, C., Cabral, A.P., 1998. The influence of tidal action on porewater nitrate concentration and dynamics in intertidal sediments of the Sado Estuary. Estuaries 21, 635. https://doi.org/10.2307/1353301.
Serôdio, J., Paterson, D.M., 2021. Role of Microphytobenthos in the Functioning of Estuarine and Coastal Ecosystems, pp. 1–13. https://doi.org/10.1007/978-3-319-71064-8_11-1.
Slomp, C.P., Epping, E.H.G., Helder, W., Raaphorst, W. van, 1996. A key role for iron-bound phosphorus in authigenic apatite formation in North Atlantic continental platform sediments. J. Mar. Res. 54, 1179–1205. https://doi.org/10.1357/0022240963213745.
Smaal, A.C., Nienhuis, P.H., 1992. The eastern Scheldt (The Netherlands), from an estuary to a tidal bay: a review of responses at the ecosystem level. Neth. J. Sea Res. 30, 161–173. https://doi.org/10.1016/0077-7579(92)90055-J.
Smaal, A.C., Schellekens, T., van Stralen, M.R., Kromkamp, J.C., 2013. Decrease of the carrying capacity of the Oosterschelde estuary (SW Delta, NL) for bivalve filter feeders due to overgrazing? Aquaculture 404 (405), 28–34. https://doi.org/10.1016/j.aquaculture.2013.04.008.
Smeaton, C., Austin, W.E.N., 2022. Quality not quantity: prioritizing the management of sedimentary organic matter across continental shelf seas. Geophys. Res. Lett. 49 https://doi.org/10.1029/2021GL097481.
ten Brinke, W.B.M., 1994. Hydrodynamic and geomorphological changes in the tidal system. In: The Oosterschelde Estuary (The Netherlands): A Case-Study of a Changing Ecosystem. Springer Netherlands, Dordrecht, pp. 15–16. https://doi.org/10.1007/978-94-011-1174-4_2.
van Zanten, E., Adriaanse, L.A., 2008. Verminderd getij, verkenning naar mogelijkheden om het verlies van platen, slikken en schorren in de Oosterschelde te beperken.
Wetsteyn, L.P.M.J., Duin, R.N.M., Kromkamp, J., Latuhihin, M.J., Peene, J., Power, A., Prins, T., 2003. Verkenning draagkracht Oosterschelde. Rijksinstituut voor Kust en Zee/RIKZ.
Wetsteyn, L.P.M.J., Kromkamp, J.C., 1994. Turbidity, nutrients and phytoplankton primary production in the Oosterschelde (The Netherlands) before, during and after a large-scale coastal engineering project (1980–1990). Hydrobiologia 282–283, 61–78. https://doi.org/10.1007/BF00024622.
Woodward, F.I., 2007. Global primary production. Curr. Biol. 17, R269–R273. https://doi.org/10.1016/j.cub.2007.01.054.
Ysebaert, T., van der Hoek, D.-J., Wortelboer, R., Wijsman, J.W.M., Tangelder, M., Nolte, A., 2016. Management options for restoring estuarine dynamics and implications for ecosystems: a quantitative approach for the Southwest Delta in The Netherlands. Ocean Coast Manag. 121, 33–48. https://doi.org/10.1016/j.ocecoaman.2015.11.005.
Zwarts, L., Blomert, A.-M., Bos, D., Sikkema, M., n.d. Exploitation of Intertidal Flats in the Oosterschelde by Estuarine Birds A&W Report 1657.